Applied Catalysis B: Environmental 172–173 (2015) 7–17

Contents lists available at ScienceDirect

Applied Catalysis B: Environmental

journal homepage: www.elsevier.com/locate/apcatb

# Supporting of pristine $TiO_2$ with noble metals to enhance the oxidation and mineralization of paracetamol by sonolysis and sonophotolysis

Asu Ziylan-Yavas[a], Yoshiteru Mizukoshi[b], Yasuaki Maeda[c], Nilsun H. Ince[a,*]

[a] Institute of Environmental Sciences, Boğaziçi University, 34342 Bebek, Turkey
[b] Kansai Center for Industrial Materials Research, Institute for Materials Research, Tohoku University, Naka-ku, Sakai, Osaka 599-8531, Japan
[c] Research Organization for University-Community Collaborations, Osaka Prefecture University, Sakai, Osaka 599-8531, Japan

ARTICLE INFO

*Article history:*
Received 7 November 2014
Received in revised form 4 February 2015
Accepted 10 February 2015
Available online 11 February 2015

*Keywords:*
Paracetamol
Immobilization
Nanocomposite
$e^-h^+$ pair
Noble metal
Photon-competition

ABSTRACT

Pharmaceutical residues in fresh water bodies are of significant environmental concern due to their undesirable effects on aquatic organisms at very low concentrations. The present study is about the elimination and overall degradation of a common anti-inflammatory pharmaceutical-paracetamol (PCT) in water by catalytic oxidation using high-frequency ultrasound, UV-irradiation (254 nm) and both. The catalysts were synthesized sonolytically by the reduction of Pd and Au to the zero-valent state followed by immobilization of the nanoparticles on the surface of commercial $TiO_2$ (P-25) to improve the activity of the semiconductor under ultrasonic and UV irradiation. It was found that sonolytic oxidation of PCT during catalysis with Pd–$TiO_2$ and Pd/Au–$TiO_2$ was very effective owing to the significantly smaller size of these particles (than that of Au–$TiO_2$), which promoted the formation and collapse of cavitation bubbles on their surface and the incidence of solute contact with the active sites. The addition of persulfate further enhanced the rate of PCT decay, signifying the role of ultrasound in activating the reagent and that of radical-initiated oxidation reactions in the decomposition of the parent compound. The activity of P-25 was low and almost equal under sonolysis and photolysis, but considerably higher under sonophotolysis, where the unfavorable properties of the semiconductor were minimized via combined effects of the two processes. Hybridization also induced a considerable synergy in carbon-mineralization, which was relatively low with single processes. The results were attributed to minimization of electron-hole pair recombination, surface corrosion and competition for photons and radical species. Au-supported particles exhibited higher activity in the presence of UV-irradiation than ultrasound, which was attributed to the unique activity of gold in the UV–vis region. Finally, Pd–$TiO_2$ was found to be the most stable nanocomposite in terms of the ease of recovery and the efficiency of reuse.



## 1. Introduction

Paracetamol (PCT) or para-acetylaminophenol-acetaminophen is a widely used analgesic/antipyretic medicine and placed among the top 200 prescriptions in the USA (2003) [1]. Despite its safety at therapeutic dosages, the medicine may be fatal at higher doses via oxidative transformation of the parent compound to *N*-acetyl-p-benzoquinone-imine (NAB), which is a toxic compound leading to hepatic necrosis [2]. Moreover, NAB is unstable in solution and hydrolyzes readily to another toxicant-1,4-benzoquinone that is also of major concern [3]. Keeping in mind that 58–68% of PCT is excreted from the body during therapeutic use [4], regulation of the parent compound and its metabolites in water (by setting maximum allowable levels) is of utmost significance to minimize its undesired health effects in potable water. Some of the recently detected concentrations of PCT in various water compartments are 6 $\mu g\,L^{-1}$ (European sewage treatment plant effluents), 10 $\mu g\,L^{-1}$ (natural waters in USA), and >65 $\mu g\,L^{-1}$ (Tyne river, UK) [5–7].

Owing to the fact that the discharge of pharmaceuticals to sewage treatment facilities is uncontrollable, the most reasonable way of regulating their presence in natural waters is by developing feasible technologies that enable their easy and environmentally safe elimination from sewage plant effluents. As such, current research on the destruction of pharmaceuticals in various water compartments has focused on advanced oxidation processes (AOPs), e.g., electrochemical oxidation [8–10],

* Corresponding author. Tel.: +90 212 3597038; fax: +90 212 2575033.
*E-mail address:* ince@boun.edu.tr (N.H. Ince).

http://dx.doi.org/10.1016/j.apcatb.2015.02.012
0926-3373/

Fenton/photo-Fenton [11–14], catalytic ozonation [15,16], UV/$H_2O_2$ [17], photocatalysis [18,19] and single or catalytic sonolysis [20–22]. Among all, those involving natural or inexpensive catalysts in solid form or slurries is very attractive due to the benefits of heterogeneous chemistry and hybridization.

One of the most widely investigated catalysts in water and wastewater remediation is powdered $TiO_2$, which is preferred for its low cost, chemical stability, non-toxicity and strong redox properties that promote oxidation, reduction and mineralization of organic compounds at the metal surface and/or within the solid–liquid interface [23]. The redox potential of $TiO_2$ arises from its ability to undergo excitation under external energy sources to produce highly energetic electron–hole pairs ($e^-h^+$). However, under conventional ambient conditions a large fraction (90%) of $e^-h^+$ species recombines within a nanosecond of their generation, and only a few are able to migrate to the metal surface for the production of reactive oxygen species such as $^\bullet OH$, $^\bullet O_2^-$, $H_2O_2$ and $^\bullet OOH$ [24].

The majority of research on $TiO_2$-based AOPs is related to the photocatalytic activity of the semiconductor despite the criticisms on its low efficiency based on high excitation band gap energy, rapid combination of the active species and limitations on its immobilization [25]. Recently however, it has been demonstrated that the band gap energy of $TiO_2$ can be effectively reduced by immobilizing it with transition metal additives, noble and rare earth metals/non-metals or with other semiconductors [26]. The technique provides extended activity of the particles in the UV–vis band via inhibition of $e^-h^+$ recombination and evasion of photo-corrosion of the metal surface [27].

Photocatalytic activity of $TiO_2$ can also be enhanced by irradiating a solution of the metal salt with ultrasound, which upon the collapse of acoustic cavity bubbles generates very-short lived local "hot spots" with temperatures >2000 K and a light emission of a wide wavelength range [28]. Note also that these "hot spots" or extreme conditions are excellent micro-reactors, where molecules of water and volatile organics undergo thermal fragmentation to release very reactive radical species that promote oxidation/reduction of organic compounds as in advanced oxidation processes.

Moreover, ultrasonic irradiation of metallic solutions is a unique means of producing zero-valent nano-metals, which upon further sonication in the presence of a semiconductor are easily immobilized on the surface with the outcome of enhanced photocatalytic activity [29]. The process is based on the formation of reducing species and the effective stirring of the slurry by the jets of liquids and shock waves that form in heterogeneous solutions during sonication [30]. It has been reported that sonolytically immobilized $TiO_2$ nanoparticles not only have very active, clean and large surfaces, but also are more homogeneously dispersed than those prepared by other techniques [31]. A summary of chemical reactions taking place during sonochemical immobilization of noble metals are given in (1–6) [32]:

$$H_2O + ))) \rightarrow {}^\bullet OH + {}^\bullet H \quad (1)$$

$$RH + {}^\bullet OH({}^\bullet H) \rightarrow \text{reducingspecies} + H_2O(H_2) \quad (2)$$

$$RH + ))) \rightarrow {}^\bullet R + \text{unstableproducts} \quad (3)$$

$$M^{+n} + \text{reductants} \rightarrow M^0 \quad (4)$$

$$nM^0 \rightarrow (M^0)_n \quad (5)$$

$$M^0 + (M^0)_n \rightarrow (M^0)_{n+1} \quad (6)$$

where:))), $M^{n+}$ and RH represent acoustic cavitation, a noble metal ion and an organic additive (essential for enhancing the production of reducing species), respectively. The reaction sequence shows that there are two sources of reductant generation, namely pyrolysis of water and RH, and abstraction reaction of RH with $^\bullet OH$ or $^\bullet H$. As a result, the noble metal ion is reduced to the zero-valent state, which upon adsorption on $(M^0)_n$ is transformed to the nano-sized form $(M^0)_{n+1}$. Note also that sonication is very suitable for the production of bi-metallic nanocomposites with the outcome of peculiar electronic, optical and catalytic properties that are absent in monometallic ones [33].

The use of precious metals such as Pt, Pd, Ag and Au has lately emerged as a promising option for immobilizing $TiO_2$ owing to the high Schottky barriers of these metals that inhibit recombination of $e^-h^+$ pairs by acting as $e^-$ traps or by promoting interfacial charge transfer processes [34,35]. The result is not only enhancement in the catalytic activity, but also benefits such as easier recovery of the metal from solution, reduced energy consumption, lower rate of surface corrosion and modifications in mechanical, optical, magnetic and electronic properties of the semiconductor [31,36].

Palladium, gold and platinum are three of the most suitable precious metals to produce nanocomposites of $TiO_2$, the excess activity of which is directly related to the degree of metal-support interactions and inversely to the metal crystal size [37,38]. An additional benefit of gold is its activity in the UV–vis region, which is expected to extend the active spectrum range of the nanocomposite [39–41]. It is also possible by sonolysis to produce bimetallic nanocomposites such as Au/Pd–$TiO_2$ with an average diameter of less than 10 nm, a Pd-shell less than 2 nm thick (a few layers of palladium atoms), and a remarkable catalytic activity arising from the inhomogeneous distribution of electrons via localization of photogenerated electrons in the Au-core [31].

The majority of research on photocatalytic degradation of PCT with $TiO_2$ reports the downside of the process for long irradiation times (at around 365 nm), high catalyst concentrations (500–2000 mg $L^{-1}$) and poor mineralization efficiency [19,42,43]. There are almost no studies on the use of $TiO_2$ nanocomposites for PCT degradation except a single one that reports complete mineralization after 1-h electrolysis of the solution (with a carbon electrode) in the presence of a $TiO_2$ nanocomposite containing CuO and $Al_2O_3$ [44].

The literature on sonocatalytic degradation of PCT is also limited, and the most interesting studies are those related to the use of hybrid processes such as US/UV/$TiO_2$, US/AC/bio-char and US/CNT [45,46], where AC and CNT refer to activated carbon and carbon nanotubes, respectively. Nevertheless, there are no studies so far that report the degradability of PCT in the presence of a mono or bi-metallic nanocomposite of $TiO_2$ supported by precious metals and activated by US or a combination of US and UV irradiation.

The present study aims to investigate the degradation of PCT by sonolysis (861 kHz), photolysis (254 nm), sonocatalysis and sono-photocatalysis using metal-supported nanocomposites of $TiO_2$ (Pd-, Au- and Pd/Au-). The impact of the metals was assessed by monitoring the activity of the nanocomposites and pristine $TiO_2$ in the decomposition and mineralization of the target compound under each test process. The study also highlights the effect of persulfate addition, the reusability performance of the composites and the synergy of the hybrid process (ultrasound/photolysis) with emphasis on the properties of the solids and the supporting metals.

## 2. Materials and methods

Paracetamol sulfate potassium salt was purchased from Sigma with >97% purity and used for preparing a standard solution of the compound. PCT test samples were prepared using 500 mg of commercially available tablet pills. The chemical structure and some of the physical/environmental properties of the product are as given [45]:

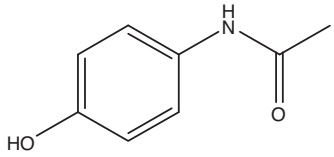

MW: 151.17 g mol$^{-1}$, $pK_a$: 9.4, Solubility: 14 g L$^{-1}$ (25 °C), log Kow: 0.46

A stock solution of PCT was made by grinding and dissolving a pill tablet in pure water at 50 °C during magnetic stirring. The solution was filtered and adjusted to pH 9.5 with NaOH to keep it stable. The concentration of PCT in the stock was determined via calibration with a standardized solution. HPLC-grade methanol, reagent grade NaOH, $H_2SO_4$, KHP were all purchased from Merck (Istanbul) and sodium persulfate from Sigma. $Na_2PdCl_4{\cdot}3H_2O$, $TiO_2$ (Degussa P-25) and polyethylene-glycol monostearate (PEG-MS) were obtained from Wako (Japan).

### 2.1. Preparation of the catalysts

Nanocomposites (Pd–$TiO_2$, Au–$TiO_2$ and Pd/Au–$TiO_2$) were synthesized sonolytically using $Na_2PdCl_4{\cdot}3H_2O$, $Na(AuCl_4)^{\bullet}2H_2O$ and powdered $TiO_2$ (Degusa P-25) in a multi-wave ultrasonic bath with a frequency of 200 kHz and a power intensity of 6 W cm$^{-2}$ (Kaijo, 4021, Japan). The procedure comprised of the following steps: (i) mixing of 1 mM of each metal salt with 0.4 mM PEG-MS (polyethylene-glycol monostearate) in 60 mL of ultrapure water followed by purging of the solutions with Ar for 10 min (in bimetallic solutions, the ratio of Au:Pd was kept at 50%:50% by molar); (ii) sonication of noble metal/PEG-MS solutions for 60 min under Ar atmosphere; (iii) addition of 8 mmol, 15 mmol and 22.5 mmol $TiO_2$ to each solution followed by sonication again for 30 min during air bubbling; (iv) separation of the nanocomposites via filtration through 0.2 μm membrane-Milipore (OmniPore) followed by washing with pure water and drying at constant temperature (60 °C) for 12 h.

For the silent adsorption tests the nanocomposite was further treated by mixing a small sample with 20 mL water and sonicating the suspension for 3-min in a water bath (35 kHz) to enhance particle stability against agglomeration thus to increase the adsorption properties of the catalysts.

### 2.2. Adsorption tests

Batch adsorption tests were carried out at varying concentrations of the catalysts (1 mg L$^{-1}$, 2.5 mg L$^{-1}$, 5 mg L$^{-1}$, 10 mg L$^{-1}$, 25 mg L$^{-1}$ and 50 mg L$^{-1}$) in a Julabo SW22 shaker at pH 3.0, 5.3 (natural pH of test solutions), 6.5 and 10.0 for 24-h to to assess the effect of catalyst dose and pH on the degree of PCT adsorption and to optimize the equilibrium conditions. The concentration of PCT and the rate of mixing were fixed at 35 μM and 250 rpm, respectively.

### 2.3. Sonolysis/sonocatalysis

Sonication of the test solution was carried out in a 500 mL glass cell equipped with a multi-frequency piezo-electric transducer (22 cm$^2$) and a 120 W generator (Ultraschall/Meinhardt, Germany). The volume of the solution was 250 mL and the power intensity (at 861 kHz) was determined by calorimetry as 1.14 W cm$^{-2}$ [46]. The optimum values of PCT concentration, frequency and pH were determined based on the rate of PCT degradation at various test levels of each parameter. The effective catalyst concentration was selected by adding 1, 2.5, 5, 10 and 50 mg L$^{-1}$ of each to the selected optimum concentration of PCT while monitoring the concentration of the compound during 60-min sonication. The experiments were repeated in the presence of commercial $TiO_2$-Degusa to assess the effect of immobilization.

The impact of persulfate addition was tested by monitoring the concentration of PCT in the presence of 5 mg L$^{-1}$ of the catalysts and various concentrations of the reagent (0.5–5.0 mM). Control experiments were run with persulfate/ultrasound in the absence of the catalysts.

### 2.4. Photolysis/photocatalysis/sonophotocatalysis

Photolytic and photocatalytic experiments were carried out by 1-h irradiation of a PCT sample solution in the absence and presence of 5 mg L$^{-1}$ of each catalyst using a low press Hg-UV lamp emitting at 254 nm. The light fluence in solution was determined by using the peroxydisulfate actinometer as 107.4 W cm$^{-2}$ [47]. The optimum pH was selected by monitoring the concentration of PCT during sonocatalysis at pH 3.0, 5.3 and 6.5 and estimating the reaction rate constant. Sonophotocatalytic experiments were also run in the sonoreactor described above and the same UV source under the optimized conditions.

All experiments with PCT (sono, photo, sono-photo, sono-PS) were run with three replicates to assess data reliability, and the pH of the solution was monitored throughout the reaction time to assess the progress of the oxidation process. The reliability of the experimental data was very good as determined by statistical analysis of replicate data ($F$ = 0.0003, $p$ = 0.99, SS = 0.000062, MS = 0.00003, STD = 0.001–0.01, variance = 0.1).

### 2.5. Stability of the catalysts

Following 40-min sonolysis of PCT with each synthesized catalyst (not exposed to post-treatment), the remaining solution was adjusted to pH 12 and kept inert for 1 h to allow desorption of organic material from the surface of the catalyst. The spent catalyst was then separated under vacuum by membrane filtration, washed with hot water, dried at 60 °C for 12 h and reused in another sonocatalytic run. The procedure was repeated three times to allow four consecutive uses of the catalyst in order evaluate its reusability. The initial concentration of PCT in each use was adjusted so as to maintain an equivalent mass ratio of PCT to catalyst at all times.

Separation of post-treated catalysts (3-min post-sonication in a bath) by the same technique was not possible due to the strong resistance of the particles to destabilization and collection on the filter surface. Other techniques such as desorption followed by evaporation and centrifugation were also tested, but the overall recovery was always lower than that obtained with non-treated catalysts.

### 2.6. Analytical

PCT was analyzed by HPLC using a Shimadzu LC-20AT HPLC with a 20A UV–vis photo diode array detector set at 220 nm, and equipped with Inertsil ODS-3V (C18) (Hypersil BDS), 250 × 4.6 mm, 5 μm particle size column. The mobile phase consisted of 25:75 methanol:water flowing at 1 mL min$^{-1}$. Sample injection volume and retention time were 10 μL and 3.45 min, respectively. Total organic carbon (TOC) was monitored by a Shimadzu TOC-V CSH analyzer after filtration of the samples through a 0.45 μm membrane filter. The concentration of hydrogen peroxide was analyzed spectrophotometrically at 351 nm using potassium iodide method [48] to select the optimum frequency of ultrasound and to assess the efficiency of OH radical ejection to solution. to select the optimum frequency of ultrasound and to assess the efficiency of OH radical ejection to solution. The decomposition of $S_2O_8^{2-}$ via activation with ultrasound was determined spectrophotometrically (UNICAM, Heλios α-Double Beam) in samples collected from the reactor at given time intervals during 30-min sonication. The method was based on the reaction of $S_2O_8^{2-}$ with $Fe^{2+}$ to form $SO_4^{-}$

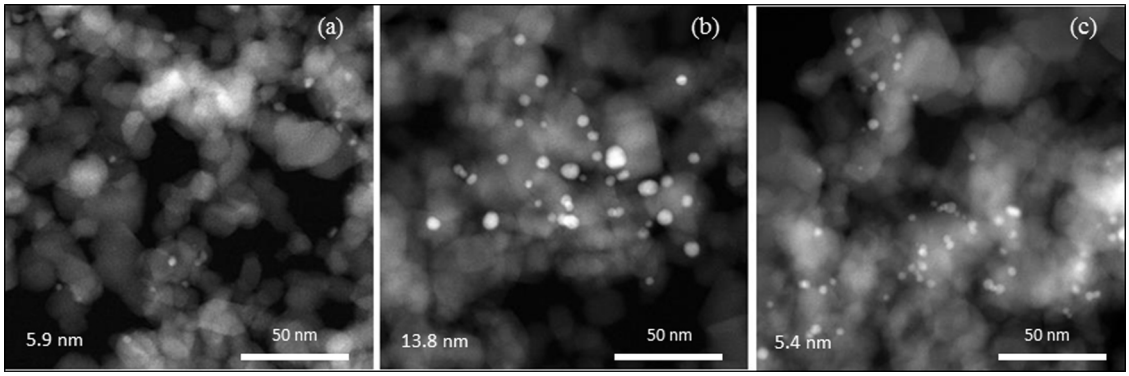


**Fig. 1.** HAADF-STEM images of (a) Pd-$TiO_2$, (b) Au-$TiO_2$, (c) and Pd/Au-$TiO_2$.

and $Fe^{3+}$ and subsequent formation of ferric cyanate $[FeSCN]^{2+}$ upon the addition of ammonium thiocyanate [49]. The formation of sulfate radicals was verified by adding 2.5 mM *t*-butanol to a test solution spiked with 2.5 mM persulfate and monitoring the evolution of $H^+$ during 40-min sonication. The method is based on the stoichiometry of t-butanol reaction with $SO_4^{-\bullet}$ to generate $H^+$ [47]. The interference of US-generated •OH with the target reaction was taken into account by monitoring the pH of a control solution during sonolysis of *t*-butanol in the absence of $S_2O_8^{2-}$. Concentrations of hydroquinone and benzoquinone (two common $TiO_2$-based catalytic oxidation byproducts of phenolic compounds) were determined by spectrophotometry in samples collected from the reactor at $t = 0$, 10, 30, 40 sand 60-min in accordance with the method described by Su et al. [50].

The structure, morphology and size of commercial and synthesized particles were analyzed by environmental scanning electron microscope (ESEM)-Philips XL30 ESEM-FEG/EDAX equipped with an SE detector. Multi-element mapping (EDX MEM/Line Scanning/Particle) and phase analyses (SUTW-Sapphire detector- EDAX ZAF Quantification) were carried out to detect, characterize and classify the indefinite features under low/high vacuum conditions without limitation (kV:15, resolution:139.70, Lsec:47–49, take-off:35.21–35.23). Nanocomposites were further analyzed by scanning-transmission electron microscopy (STEM, FEI Titan 80–300 operated at 300 kV) equipped with a large-angle annular dark field (HAADF) detector to obtain more precise information on particle sizes less than 10 nm. The beam convergence and inner angles of HAADF detector were 10 mrad and >60 mrad, respectively. Hydrodynamic diameter and size distribution analyzes were made in dilute solutions of the particles using a Brookhaven 90-Plus nanoparticle size analyzer operated with the method of dynamic light scattering (DLS).

The band gap energies of $TiO_2$ and the nanocomposites were determined by recording the UV-diffuse reflectance spectra of the solids (200–600 nm) using a UV–vis spectrophotometer (UV-2450, Shimadzu) equipped with an integrating sphere reflectance accessory. The data were evaluated by reference to Kubelka–Munk (KM) transformations and linear extrapolation of the diffuse reflectance spectra as described in the literature [51].

## 3. Results and discussion

### 3.1. Characterization of nanocomposites

SEM analysis of catalyst surfaces for chemical layer characterization and homogeneity showed that neither the noble metals nor $TiO_2$ were concentrated in any specific area of the composite surface signifying a uniform dispersion, i.e., the metals were homogeneously distributed throughout the $TiO_2$ surface with no particle aggregation (the images obtained by multi-element mapping are provided in Fig. S1). Particle size analysis by SEM showed that the size of P-25 or $TiO_2$-Degussa was between 30–40 nm, which is consistent with the data reported by the current manufacturer (Evonik), that of Au–$TiO_2$ was around 14–20 nm, and those of Pd–$TiO_2$ and Pd/Au–$TiO_2$ were less than 10 nm. As such, STEM analysis was used to acquire higher resolution images that allow determination of the exact size, composition and localization of the metals on the nanocomposites. The images obtained are depicted in Fig. 1(a–c), for Pd–$TiO_2$, Au–$TiO_2$ and Pd/Au–$TiO_2$, respectively. The brighter spots in the first two represent Pd and Au immobilized on $TiO_2$; the brighter core and the darker shell in the last one signify locations of the heavier Au and the lighter Pd, respectively in accordance with the interpretation of STEM images of bimetallic nanocomposites, as reported previously [31]. The average particle size in Au–$TiO_2$, Pd–$TiO_2$ and Pd/Au–$TiO_2$ was 13.8 nm, 5.9 nm and 5.4 nm, respectively.

The band gap energies of all particles were found to be the same at around $3.25 \pm 0.01$ eV, and the result was attributed to the absence of doping agents that would generate new energy levels between the valence band and the conduction band.

### 3.2. Silent adsorption of PCT on $TiO_2$ and/or its nanocomposites

Silent adsorption tests revealed that equilibrium was reached at around 6-h with all of the catalysts and the highest fraction of PCT accumulation after 24 h was on Au–$TiO_2$ as 17% at pH 6.5, implying that adsorptive elimination of the compound under these conditions was insignificant. The data are presented in Fig. 2(a) for commercial and post-treated nanocomposites, the adsorptive properties of which were slightly better than that of the original untreated portion (via improved particle stability that inhibited agglomeration).

It was found that the value of pH that provided maximum adsorption on the surface of the catalysts was 6.5, most likely because the surface of $TiO_2$ is slightly positive at pH < zero point charge (6.8), at which PCT is neutral (nonionic state) and poorly soluble ($pK_a = 9.4$) so that there is practically no repulsion between the solute and the solid surface. In accordance, acidic pH was less favorable due to increased electrostatic repulsion between protonated molecules of the compound and the positively charged adsorbent surface. Note also that no adsorption was observed at pH 10 (data not shown) due to the negative charge on the surface of the solids and the anionic form of the compound at pH > $pK_a$.

We also observed that the fraction of PCT adsorbed was remarkably increased when the adsorbent concentration was 50- and 100-fold increased as depicted in Fig 2(b) for post-treated Pd–$TiO_2$. The adsorption equilibrium and the corresponding Lang-

muir isotherm parameters for the same catalyst are provided in Fig. S2.

### 3.3. Sonolysis and sonocatalysis

The optimum conditions of frequency, PCT concentration and pH by ultrasonication alone were selected (based on maximum rate of degradation and carbon-mineralization) as 861 kHz, 35 μM and 3.0, respectively, as shown in Fig. 3(a–d). Higher reactivity under acidic conditions, lower solute concentrations and the selected frequency had been discussed thoroughly in the past with emphasis on the ability of solutes to diffuse to the bubble–liquid interface, reduced competition for radical species, and higher incidence of •OH ejection to the bulk solution, respectively [52–54]. Hence, the degradation of PCT by sonolysis was realized by •OH-mediated oxidation reactions mostly in the bulk liquid and partly at the bubble-liquid interface, where the concentration of •OH is very high. It was also found that the rate of degradation in most cases deviated from the pseudo-first order law and fitted perfectly to the following expression:

$$\frac{C}{C_0} = e^{-kt} + \delta \quad (7)$$

where, $C$ and $C_0$ are concentrations of PCT at time $t$ and zero, respectively, $k$ is the apparent reaction rate constant (time$^{-1}$) and $\delta$ is the deviation factor that is equal to a non-zero plateau representing the ultimate value of $C/C_0$. In fact, a plot of $\ln(C/C_0)$ against time for a sonochemical reaction usually ends up with two straight lines: the steeper one represents the rapid decay of the solute at early reaction while the other is responsible for the rest of the time, as typical of heterogeneous reaction systems (e.g., gas–liquid heterogeneity in sonicated water) with exhausting sites of adsorption.

Sonication of PCT in the presence of the catalysts showed that previously optimized values of solute concentration and frequency could be kept at the optimized levels, but the value of pH needed re-optimization due to faster degradation of the compound at near neutral pH than at acidic. The effect of pH on the degradation ($t$ = 40-min) and mineralization ($t$ = 60-min) of PCT by sonolysis in the presence of Pd–$TiO_2$ are presented in Fig 4(a–c). Note that at acidic pH the rate of PCT decay is slower than that obtained by sonication without catalysts to be attributed to ineffective transport of PCT molecules to the catalyst surface, which contains reactive oxygenated species as well as $e^-h^+$ pairs. Higher reactivity at pH 6.5 is the consequence of better adsorptive properties, as also observed in silent adsorption experiments. Note also that the reaction rate in this process also deviated from the pseudo-first order law and the relation between the initial rate and PCT concentration confirmed Langmuir–Hinshelwood type of kinetics. Two-region decay pattern and the fit of Langmuir–Hinshelwood rate expression to the data are presented in Fig. S3. This and the fact that there existed multiple interfaces in our system (gas–liquid, gas–solid, solid–liquid) we were justified in expressing the fraction of concentration decay with time by Eq. (7).

It was also found that the rate of PCT decay was very sensitive to the mass of catalyst in the reactor, increasing within a low concentration range (1–10 mg L$^{-1}$) and declining at higher loadings, as depicted in Fig. 4(d). Such a rate pattern is the sign of adsorption-mediated reactions and implies the presence of too many noble metals at high loadings that partially block the surface of $TiO_2$ (or hinder the adsorption of •OH on the surface). Another factor that may be responsible for the slower reactions is agglomeration of particles at high concentrations (despite the effect of ultrasound to disaggregate) that leads to reduced efficiency of energy transmission and attenuation of the ultrasonic field. The tendency for agglomeration was confirmed by the zeta potentials of the composites, as depicted in Fig. S4.

Relative efficacy of all catalysts for the decomposition and mineralization of PCT by sonocatalysis is presented in Fig. 5. The data show that catalytic activity increased with decreasing particle size and the most effective catalysts during the oxidation and mineralization processes were Pd–$TiO_2$ and Pd/Au–$TiO_2$, respectively. The superiority of Pd is believed to arise from its high surface energy, which enables a more efficient contact between the metal and the oxygen vacancies on the surface of $TiO_2$ [55]. Moreover, noble metals such as Pt and Pd are reported to increase the acidic strength of catalyst surfaces, thus, improving the adsorption efficiency of solutes [56].

The biphasic character of PCT decay in the presence of Pd–$TiO_2$ (very fast only during the first 10-min and slower, thereafter) justifies why it was more effective in the oxidation of PCT and less in

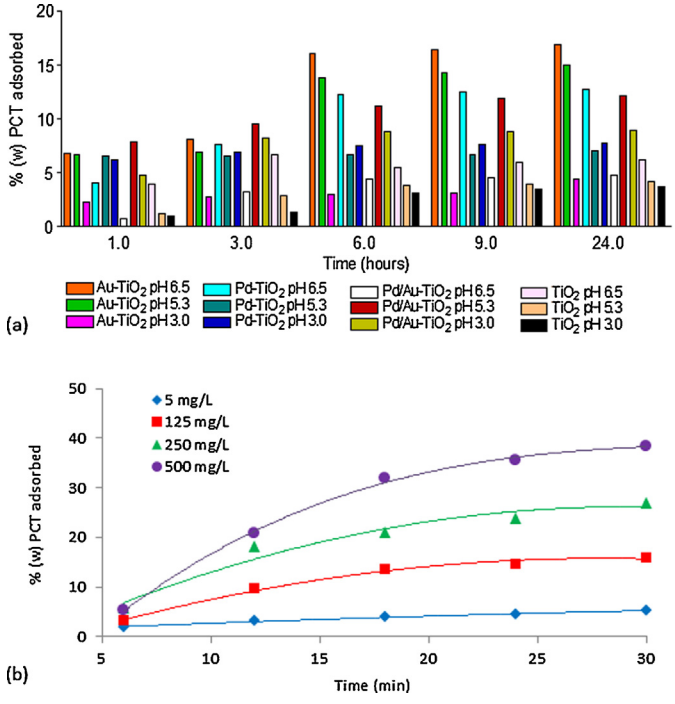


**Fig. 2.** Relative adsorption of PCT ($C_0$ = 35 μM) on 5 mg L$^{-1}$ of commercial and immobilized $TiO_2$ during silent shaking: (i) the effect of pH; (ii) the effect of increasing the adsorbent concentration (data are representative of sono-treated Pd-$TiO_2$).

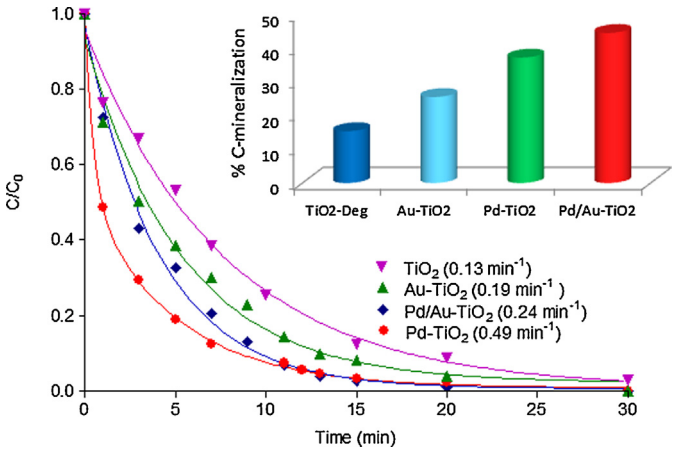


**Fig. 5.** Relative rate of PCT degradation during 30 min sonocatalysis at pH 6.5. The insert shows the decay of TOC in 1 h reaction under the same conditions: $C_0$ = 35 μM PCT, $f$ = 861 kHz, cat = 5 mg L$^{-1}$. Figures in brackets are the reaction rate constants estimated by Eq. (7).

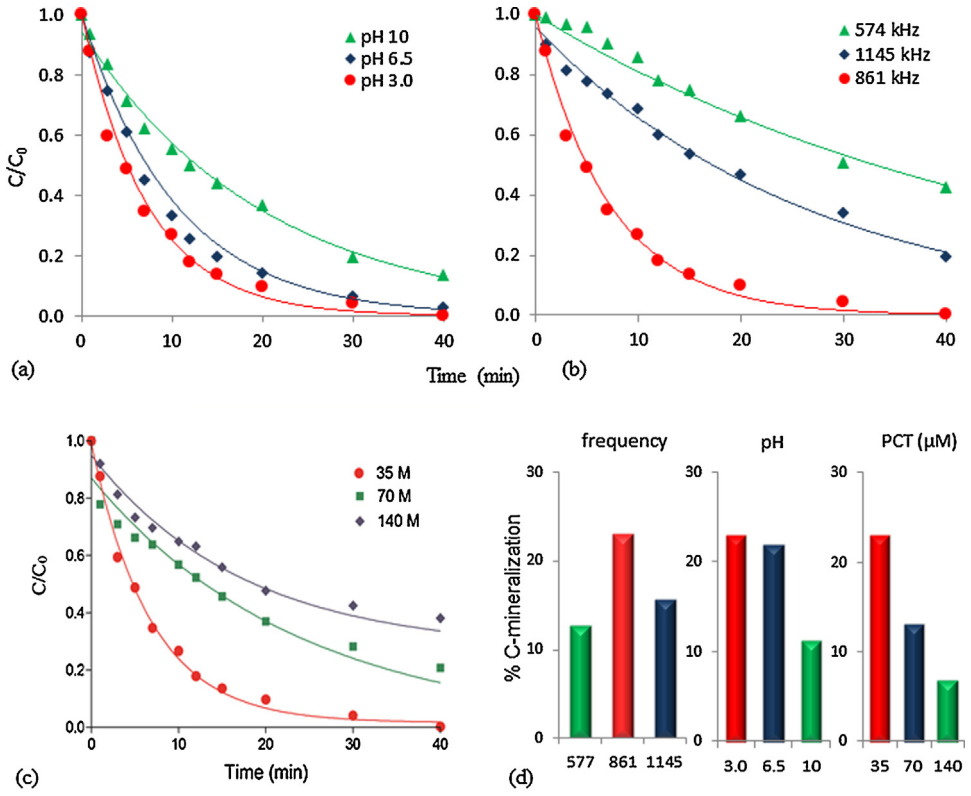


**Fig. 3.** The impact of pH, frequency, and concentration on the rate of PCT degradation (a, b, c) and C-mineralization (d) by ultrasound. The solid lines represent exponential fits of Eq. (7) to the observed data.

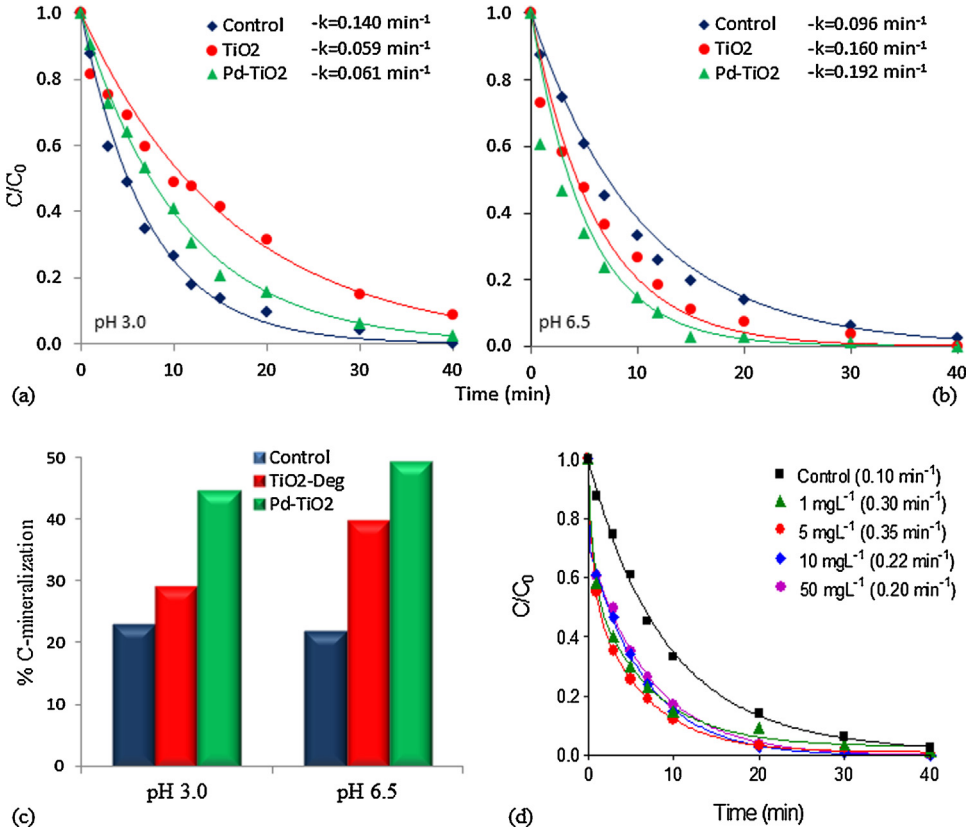


**Fig. 4.** The impact of pH on sonocatalytic degradation and mineralization of (35 μM, 861 kHz) in the presence of 5 mg $L^{-1}$ of commercial and Pd-supported $TiO_2$ (a, b, c); the effect of catalyst (Pd-$TiO_2$) concentration at pH 6.5 (d). "Control" and "$TiO_2$-Deg" refer to ultrasound alone and commercial $TiO_2$-P25 (Degussa), respectively.

mineralization (41% and 54% reduction in TOC with Pd–$TiO_2$ and Pd/Au–$TiO_2$, respectively). Such bi-phasic character also implies different selectivity of the catalyst for the parent and the oxidation compounds. Note also that both of Pd-supported particles (Pd–$TiO_2$, Pd/Au–$TiO_2$) were remarkably more effective than Au-supported counterparts as a consequence of their much smaller particle size that promoted the formation of excess cavitation nuclei and thus, the production and adsorption of excess •OH and ROS on their surface. Analysis of hydrodynamic diameters in dilute suspensions showed that smaller particles had also smaller hydrated diameters and vice versa, indicating that the activity of the catalysts in solution was reduced by increased coverage of their surface with molecules of water. The data and distribution of particle size in water are provided in Fig. S5.

### 3.4. The effect of persulfate addition

It has been previously demonstrated that persulfate ($S_2O_8^{2-}$) is an excellent reagent in AOPs via its activation to generate $SO_4^{-\bullet}$ with an oxidation potential of 2.16 eV [57] that is lower but comparable with that of the OH radical (2.83 eV). The process requires the use of heat, UV-irradiation, ultrasound or transition metal additives as demonstrated, respectively, in the following reactions [57,58]:

$$S_2O_8^{2-} + \Delta \rightarrow 2SO_4^{-\bullet} \quad (8)$$

$$S_2O_8^{2-} + h\upsilon \rightarrow 2SO_4^{-\bullet} \quad (9)$$

$$S_2O_8^{2-} + ))) \rightarrow 2SO_4^{-\bullet} \quad (10)$$

$$S_2O_8^{2-} + Me^{+} \rightarrow SO_4^{-\bullet} + SO_4^{2-} + Me^{(n+1)+} \quad (11)$$

When ultrasound is the method of activating persulfate (PS), additional benefits are obtained such as production of •OH and $H_2O_2$ via water pyrolysis, and acceleration of mass transfer and chemical reaction rates via mechanical effects of ultrasound. As such, PS was found a highly effective additive in sonochemical elimination of some refractory/toxic compounds in water [59–63]. Moreover, at neutral and alkaline conditions sulfate radical readily reacts with $H_2O$ and/or $OH^-$, respectively, to yield additional hydroxyl radicals as [64]:

$$SO_4^{-\bullet} + H_2O \rightarrow HO^{\bullet} + H^{+} + SO_4^{2-} \quad (12)$$

$$SO_4^{-\bullet} + OH^{-} \rightarrow SO_4^{2-} + HO^{\bullet} \quad (13)$$

Silent reaction of PCT with persulfate showed that the most effective concentration of the reagent was 2.5 mM, below and above which the reaction was slowed down due to the scarcity and abundance of $SO_4^{-\bullet}$, respectively (the latter leading to •OH scavenging). More significantly, the reaction was very sensitive to variations in pH, as depicted in Fig. 6. The data show that at pH 10, PCT was completely decomposed within 20-min via a zero-order reaction rate and formation of a pale yellow color. This is consistent with the literature, where direct reaction of PCT with persulfate at alkaline pH was reported to produce *p*-nitrophenol and $CH_3COOH$, the former recognized with its yellowish color [64]. However, alkaline pH was ineffective for the mineralization of PCT by persulfate, because only 4% of TOC was decomposed at the end of 1-h contact.

Considering that decomposition of the oxidation byproducts is at least as important as that of the parent compound, we conducted sonolytic experiments with persulfate at pH 6.5, which was selected as the optimum operating pH for all reactions. Before we started the experiments, we monitored the decay in the concentration of persulfate and the activity of sulfate radical by the methods described in Section 2.6. The results of these preliminary analyses (Fig. S6) showed that $S_2O_8^{2-}$ was effectively activated by ultrasound to produce sulfate radicals.

The rate of PCT elimination and (%) TOC decay by sonocatalysis in the presence of 2.5 mM PS are presented in Fig. 7(a and b), respectively. It was found that Pd–Au/$TiO_2$ and Pd–$TiO_2$ were the most effective catalysts in the oxidation and mineralization processes, respectively. Different performance of the catalysts in this and the previous process (without $S_2O_8^{2-}$) must be due to differences in the reaction byproducts and selectivity of the particles for them. Note also the remarkable improvement obtained in the performance of $TiO_2$-Degussa for mineralization (from 15% to 38%) implying the enhancement in the quantity of adsorbed radical species and a higher selectivity of the catalyst for the oxidation products.

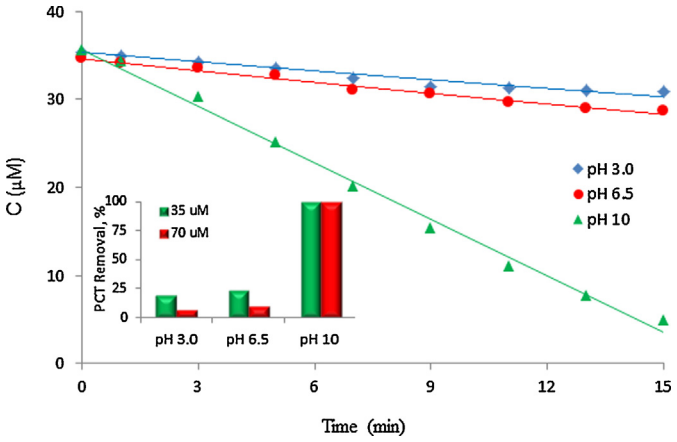


**Fig. 6.** Oxidation decay of PCT ($C_0$ = 35 μM) by 15 min reaction with persulfate (2.5 mM) under silent conditions at pH 3.0, 6.5 and 10. The inset shows the impact of PCT initial concentration on the fraction of decay after 1 h contact with PS.

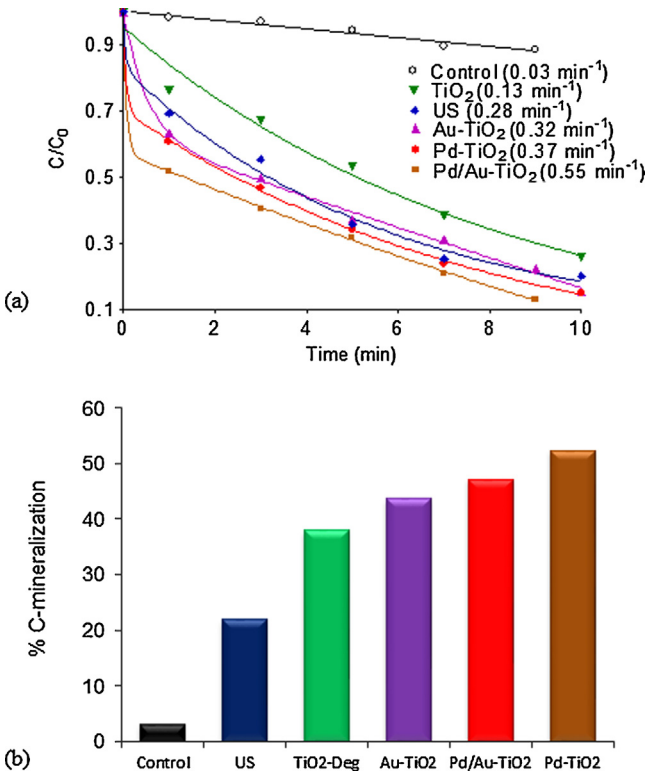


**Fig. 7.** The impact of PS addition (2.5 mM) on the initial rate of degradation (a) and 1 h mineralization of PCT (b) in the presence of ultrasound and 5 mg $L^{-1}$ of commercial and immobilized $TiO_2$ at pH 6.5. "Control" refers to PS alone; figures in brackets are 10 min reaction rate constants as estimated by Eq. (7).

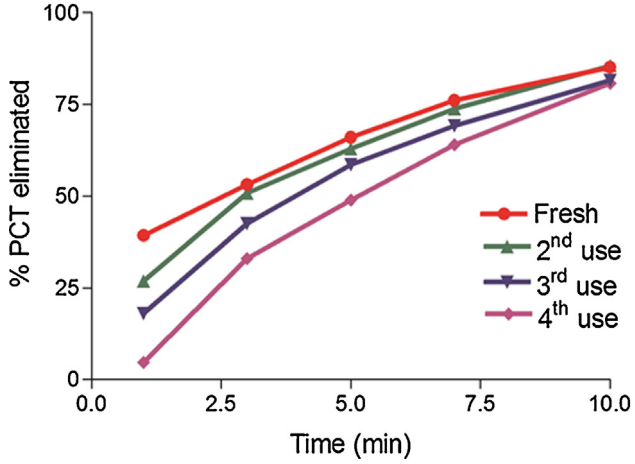


**Fig. 8.** The loss in the efficiency of Pd-$TiO_2$ upon recovery and reuse of the spent catalyst successively in sonocatalytic degradation of PCT.

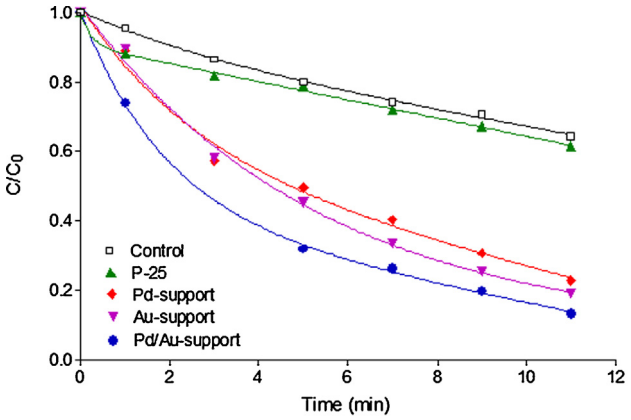


| Type of $TiO_2$ | Absorption Wavelength | A (254 nm) | A (365 nm) |
|---|---|---|---|
| P-25 | 328-358 nm | 0.105 | 0.089 |
| Pd-support | 264-372 nm | 0.175 | 0.108 |
| Au-support | 272-284 nm | 0.239 | 0.142 |
| Pd/Au-support | 328-368 nm | 0.470 | 0.325 |

**Fig. 9.** Initial rate of PCT decay by photolysis (254 nm) in the presence of 5 mg $L^{-1}$ of commercial and immobilized $TiO_2$ ("Control" refers to UV alone). The estimated rate constants are 0.09, 0.11, 0.18, 0.19 and 0.30 $min^{-1}$ for Control, $TiO_2$-Deg, Pd-$TiO_2$, Au-$TiO_2$ and Pd/Au-$TiO_2$, respectively. The table at the bottom shows the absorption properties of the particles at UVC and UVA regions.

### 3.5. Stability of the catalysts

One of the most important features of solid catalysts is their stability, i.e., the ease of recovery and the loss of efficiency upon multiple-use. In general, the higher the recovery of a spent catalyst and the lower is the loss of efficiency in the next use, the more stable and economical it is. In that sense, Pd–$TiO_2$ was found as the most stable catalyst with 84%, 72% and 69% recovery, respectively, at the end of 1st, 2nd and 3rd consecutive uses in sonocatalytic degradation of PCT. It was also found that although the activity of the spent catalyst was initially less than that in the previous run, it rapidly improved within the first 7-min and closely equalized with the original activity. Relative efficacy of the fresh and spent Pd–$TiO_2$ during 10-min reaction of PCT under ultrasonic irradiation is presented in Fig. 8.

The very good performance of the nanocomposite in recovery and reuse does not only highlight the role of ultrasound in continuous cleaning of surfaces and disaggregation of particles to allow efficient trapping of sono-generated electrons, but also implies the insignificance of dynamic changes in particle size (via leaching of the immobilized metals) with successive uses. A similar and even higher efficiency of reusability has been reported for a high-temperature annealed Au/$TiO_2$ sample, with data showing that particle densities and size distributions were indistinguishable from the fresh counterparts [65]

### 3.6. Photo- and sono-photocatalysis

The use of UVC irradiation ($\lambda_{max}$ = 254 nm) in photocatalytic experiments with the synthesized particles was found to be remarkably more effective than UVA ($\lambda_{max}$ = 365 nm) to be attributed to the dual function of the former for excitation of the catalyst surface and decomposition of the target compound. Direct reaction of PCT with UV-254 nm irradiation has also been reported in the literature and explained by the migration of the acetyl group onto the aromatic ring in o-position to the amino moeity [66]. Hence, all light-bearing experiments were carried out using the low-pressure Hg-UV lamp described in section 2.4.

We found that the rate of PCT decay by photolysis alone and photocatalysis with P-25 was the same, implying that the surface of the catalyst in commercial form was not activated by the test light source. However, the reaction was considerably faster when catalyzed by metal-supported counterparts as depicted in Fig. 9 together with the absorption properties of the catalysts. The reason for presenting these two data sets together is because the band gap energies of all particles were the same and particle size alone

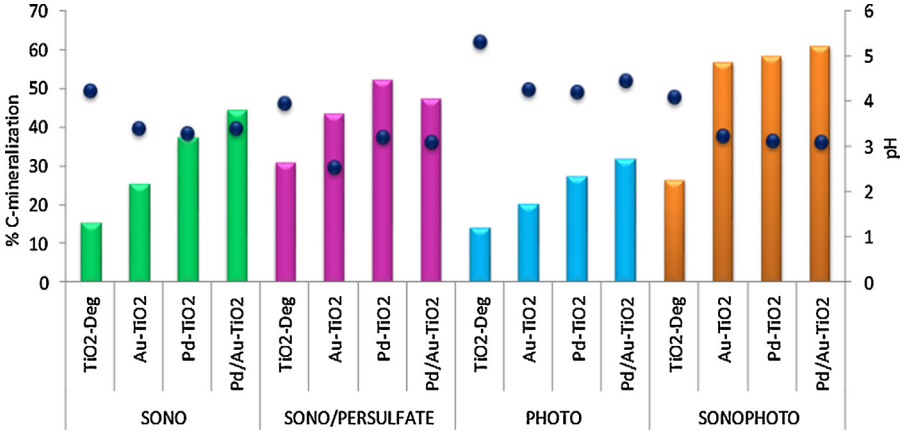


**Fig. 10.** Relative mineralization of PCT ($C_0$ = 35 μM) after 60 min exposure to the test presence of commercial and immobilized $TiO_2$ (5 mg $L^{-1}$) at pH 6.5.

**Table 1**
The apparent reaction rate constants of PCT decay (min-1) by sonolysis, photolysis and sono-photolysis and the corresponding synergy indices. The last two columns show relative mineralization efficiency of the hybrid process for each catalyst and the corresponding synergy, respectively. Initial conditions were $TiO_2$ = 5 mg $L^{-1}$, PCT = 35 μM, pH 6.5.

| Catalyst | $k_s$ | $k_p$ | $k_{sp}$ | $S_{ox}$ | (%)-Miner | $S_{Miner}$ |
|---|---|---|---|---|---|---|
| P-25 | 0.13 ± 0.03 | 0.11 ± 0.07 | 0.13 ± 0.02 | 1 | 26.41 | 1.71 |
| Au- | 0.19 ± 0.04 | 0.21 ± 0.02 | 0.25 ± 0.04 | 1.31 | 56.8 | 2.23 |
| Pd- | 0.49 ± 0.04 | 0.18 ± 0.05 | 0.65 ± 0.05 | 3.42 | 58.74 | 1.37 |
| Pd/Au- | 0.24 ± 0.09 | 0.30 ± 0.08 | 0.67 ± 0.06 | 2.8 | 61.02 | 1.58 |

was insufficient to explain the observed differences in catalytic activities.

The absorption properties in the table show that the effect of single metal support was to extend the active spectrum range of the semiconductor, while that of bi-metallic support was to enhance the intensity of absorption. Hence, much faster degradation of PCT in the presence of Pd/Au–$TiO_2$ than the other composites must be the output of very small size and largest intensity of surface absorption. Nevertheless, Au–$TiO_2$ despite its smallest size was the second most active catalyst. The paradox can be explained by the "shadowing" effect, i.e., when the size of the nanocomposite is too small as in Pd–$TiO_2$, the surface may be shadowed by the presence of too many metals on it leading to a low efficiency of light absorption [29]. Although a similar or even larger "shadowing" should be present on the surface of Pd/Au–$TiO_2$, the effect is believed to be offset by the activity of Au in the UV–vis region as reflected by the absorption intensity of the composite. Some researchers have reported that the unique role of Au in photocatalysis may also arise from its ability for surface plasmon band absorption, which enables the absorption of the nanocomposite in the same wavelength thus leading to more effective utilization of the excited electrons [67]. Finally, it should be noted that the work function of Au (promotion effect) is high enough to enhance the efficiency of trapping the photo-excited electrons on the semiconductor to restrict recombination of electron-hole pairs [29].

The final test process was sono-photocatalysis, which was expected to provide a synergy via enhanced rate of surface excitation, reduced surface corrosion and increased rate of mass transfer to the solid surfaces. The synergy was estimated by Eq. (14), where $S$ is the synergy index, $k_{SP}$, $k_S$, $k_P$ and $P_{sp}$, $P_s$, $P_p$ are the apparent reaction rate constants ($min^{-1}$) and the deposited energy (W $cm^{-2}$) in sono-photolysis, sonolysis and photolysis, respectively. Owing to variations in the activity of the catalysts in the mineralization process, we also estimated the synergy in mineralization by replacing the rate constants in Eq. (14) with % TOC decay in 1-h.

$$S = \frac{k_{SP}P_{sp}}{k_S P_s + k_P P_p} \quad (14)$$

A list of 10-min reaction rate constants and 60-min mineralization efficiencies of each test process and catalyst and the corresponding synergy indices are given in Table 1. The results show that the highest synergy in the oxidation of PCT was obtained with Pd–$TiO_2$, and no synergy was present with the commercial particles, as expected. The former is the outcome of high work function (under UV) and higher surface energy of Pd (than Au) to reduce recombination of e–h pairs [59], and to enhance the adsorption of solutes, respectively.

Surprisingly, the hybrid process was found to enhance the mineralization of PCT in the presence of all particles, but the most remarkable synergy was obtained with P-25. The implication is that the addition of acoustic cavitation to a suspension of pristine $TiO_2$ under UV-irradiation minimizes the inefficiencies of the semiconductor, such as for example rapid corrosion of the surface. Note also the high synergy obtained with Au–$TiO_2$ for mineralization that

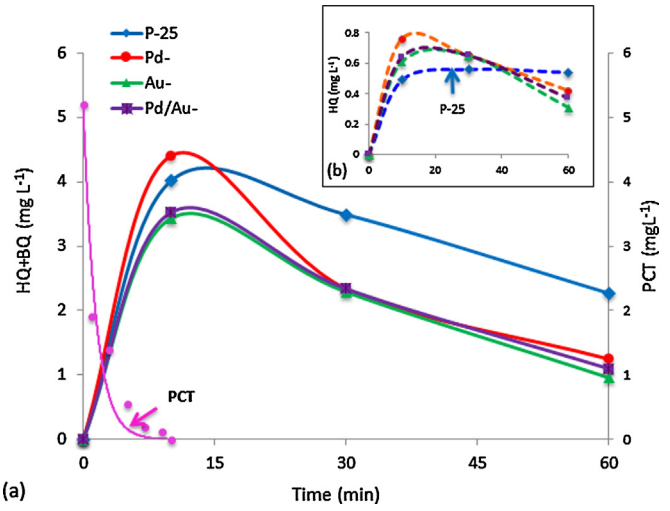


**Fig. 11.** Evolution of hydroquinone + benzoquinone (a) and hydroquinone only (b) during 60 min sonophotocatalysis of PCT. Initial conditions were: PCT = 35 μM (5.2 mg $L^{-1}$), $TiO_2$ = 5 mg $L^{-1}$, pH 6.5. The pink link shows exponential decay of PCT in the presence of Pd/Au-$TiO_2$.

could have arisen from a variety of factors such as (i) the special function of Au on $TiO_2$ for accelerating the decomposition of water and the production of hydrogen gas to provide additional oxidation and reduction pathways for the degradation of the byproducts [68]; (ii) the high work function and ability of the metal for surface plasmon band absorption, as pointed out in relation to its good performance in photolysis.

Relative efficacy of all test catalysts and processes (including sono-persulfate) for the ultimate degradation of PCT (mineralization) is presented in Fig. 10 together with the observed pH changes. The lower efficiency of photolysis (than sonolysis) has been discussed in relation to incomplete decomposition of PCT (sustained competition for photons) and the effect of shadowing induced by too many metals on the surface of the catalyst. Still another factor that may be effective is the unsuitability of the stereochemical configuration of PCT for chelating with titanium [66]. However, it should be kept in mind that the energy deposited in solution during sonolysis was more than two orders of magnitude larger (than that in photolysis), which explains why the hybrid process was highly synergistic in the mineralization of the compound. It is also true that in sono-photolysis PCT was completely eliminated within the first 7 min, so that the two unfavorable conditions of photolysis (photon competition and stereochemical unsuitability) disappeared during the mineralization process. This also implies that the oxidation byproducts were inactive under UV-C irradiation, as supported by the literature reporting non-reactivity of the primary photolysis byproducts of PCT with UV-254 nm [66].

Finally, we monitored the evolution of two common byproducts of catalytic oxidation of phenolic compounds with $TiO_2$, namely hydroquinone (HQ) and benzoquinone (BQ) during 60-min photocatalysis of PCT ($C_0$ = 5.18 mg $L^{-1}$). We found that regardless of the particle composition PCT was readily oxidized to HQ and BQ, and the sum of the byproducts increased during the first 10-min and declined, thereafter as depicted in Fig. 11-a. However, the sum of HQ and BQ at $t$ = 60 min was around 1.0 mg $L^{-1}$ for the reactions catalyzed with metal-supported $TiO_2$ and 2.3 mg $L^{-1}$ with pristine $TiO_2$. The difference implies that in the presence of the latter one or both of the compounds accumulated via inhibition of the oxidation reactions. To confirm the hypothesis we analyzed relative evolution of HQ in the presence of each catalyst, as depicted in Fig. 11-b. The data show that only in the presence of P-25 does HQ accumulate while the sum of HQ + BQ continued to decrease (Fig 11-a), implying

that a catalytic oxidation–reduction cycle between the two compounds led to undesired consumption of sono/photo-generated electrons and ROS. A similar reasoning has been reported in the literature for the low efficiency of pristine $TiO_2$ in photocatalysis and concluded that noble metals decorated on the surface of the semiconductor not only inhibited recombination of e–h pairs, but also participated in the reaction [65].

## 4. Conclusions

Decoration of noble metals on the surface of pristine $TiO_2$ is a promising method of enhancing the sonolytic and photolytic activity of the semiconductor, as demonstrated in this study via enhanced rate of PCT decomposition and mineralization in the presence of Pd-, Au- and Pd/Au-supported $TiO_2$ nanoparticles. The enhancement was related to the size of the particles and the enlargement in their surface area that allowed more efficient adsorption of solutes and larger formation/availability of cavitation bubbles, $e^-h^+$ pairs and oxygenated species. Different performance of the catalysts under ultrasound and UV irradiation was attributed to different absorption properties and work functions of the metals in the UV–vis region. Simultaneous application of ultrasound and UV-irradiation induced a remarkable synergy in the oxidation of PCT and degradation of the byproducts, signifying the role of cavitation in increasing the rate of mass transfer to heterogeneous interfaces, cleaning of solid surfaces, disaggregating of particles and minimizing undesired corrosion of the catalyst surface upon excitation by a light source. The study has also highlighted the role of persulfate in enhancing the efficiency of the processes and the superiority of Pd-supported particles in relation to their activity under ultrasonic irradiation and good performance in recovery and reuse.

## Acknowledgements

The research was funded by Boğaziçi University Research Fund through Project 12Y00D8. Synthesis of the nanocomposites was supported by JST and JICA through the project SATREPS according to the International Cooperation Program of Osaka Prefecture University, Japan. The authors are grateful to Dr. N. Ökte in the Chemistry Department of Boğaziçi University for her help in determination of band gap energies.

## Appendix A. Supplementary data

Supplementary data associated with this article can be found, in the online version, at http://dx.doi.org/10.1016/j.apcatb.2015.02.012.

## References

[1] Y. Liu, K. Wan, N. Deng, F. Wu, React. Kinet. Mech. Catal. (2010) 493–502.
[2] M. Bedner, W.A. MacCrehan, Environ. Sci. Technol. 40 (2006) 516–522.
[3] D.C. Dahlin, S.D. Nelson, J. Med. Chistry. 25 (1982) 885–886.
[4] J.S.N. Muir, J.D. Nichols, M.R. Stillings, Curr. Med. Res. Opin. 13 (1997) 491–500.
[5] D.W. Kolpin, E.T. Furlong, M.T. Meyer, E.M. Thurman, S.D. Zaugg, L.B. Barber, H.T. Buxton, Environ. Sci. Technol. 36 (2002) 1202–1211.
[6] P.H. Roberts, K.V. Thomas, Sci. Total Environ. 356 (2006) 143–153.
[7] T. Ternes, Water Res. 32 (1998) 3245–3260.
[8] E. Brillas, S. Garcia-Segura, M. Skoumal, C. Arias, Chemosphere 79 (2010) 605–612.
[9] I. Sirés, J.A. Garrido, R.M. Rodríguez, P.L. Cabot, F. Centellas, C. Arias, E. Brillas, J. Electron. Spectrosc. Relat. Phenom. Electrochem. Soc. 153 (2006) D1–D9.
[10] K. Waterston, J.W. Wang, D. Bejan, N.J. Bunce, J. Appl. Electrochem. 36 (2005) 227–232.
[11] N. Klamerth, L. Rizzo, S. Malato, M.I. Maldonado, A. Agüera, A.R. Fernández-Alba, Water Res. 44 (2010) 545–554.
[12] M.D.G. de Luna, M.L. Veciana, J.I. Colades, C.-C. Su, M.-C. Lu, J. Taiwan Inst. Chem. Eng. 45 (2014) 565–570.
[13] F. Velichkova, C. Julcour-Lebigue, B. Koumanova, H. Delmas, J. Environ. Chem. Eng. 1 (2013) 1214–1222.
[14] C.-C. Su, L.M. Bellotindos, A.-T. Chang, M.-C. Lu, J. Taiwan Inst. Chem. Eng. 44 (2013) 310–316.
[15] R. Andreozzi, V. Caprio, R. Marotta, D. Vogna, Water Res. 37 (2003) 993–1004.
[16] F. Centellas, C. Arias, M. Skoumal, A. Garrido, E. Brillas, R. Marı, Appl. Catal. B Environ. 66 (2006) 228–240.
[17] D. Vogna, R. Marotta, A. Napolitano, M. D'Ischia, J. Org. Chem. 67 (2002) 6143–6151.
[18] L. Yang, L.E. Yu, M.B. Ray, Water Res. 42 (2008) 3480–3488.
[19] E. Moctezuma, E. Leyva, C.A. Aguilar, R.A. Luna, C. Montalvo, J. Hazard. Mater. 243 (2012) 130–138.
[20] Q. Isariebel, J. Carine, J. Ulises-javier, W. Anne-marie, D. Henri, Ultrason. Sonochem. 16 (2009) 610–616.
[21] J.-K. Im, L.K. Boateng, J.R.V. Flora, N. Her, K.-D. Zoh, A. Son, Y. Yoon, Sep. Purif. Technol. 123 (2014) 96–105.
[22] J.-K. Im, J. Heo, L.K. Boateng, N. Her, J.R.V. Flora, J. Yoon, K.-D. Zoh, Y. Yoon, J. Hazard. Mater. 254–255 (2013) 284–292.
[23] J. Wang, B. Guo, X. Zhang, Z. Zhang, J. Han, J. Wu, Ultrason. Sonochem. 12 (2005) 331–337.
[24] N.N. Binitha, Z. Yaakob, R. Resmi, Cent. Eur. J. Chem. 8 (2010) 182–187.
[25] M. Ashokkumar, Int. J. Hydrogen Energy 23 (1998) 427–438.
[26] P.V. Kamat, D. Meisel, Curr. Opin. Colloid Interface Sci. 7 (2002) 282–287.
[27] J.C. Kim, J. Choi, Y.B. Lee, J.H. Hong, J.I. Lee, J.W. Yang, W.I. Lee, N.H. Hur, Chem. Commun. (Camb.) (2006) 5024–5026.
[28] N. Shimizu, C. Ogino, M.F. Dadjour, T. Murata, Ultrason. Sonochem. 14 (2007) 184–190.
[29] Y. Mizukoshi, Y. Makise, T. Shuto, J. Hu, A. Tominaga, S. Shironita, S. Tanabe, Ultrason. Sonochem. 14 (2007) 387–392.
[30] K.S. Suslick, G.J. Price, Annu. Rev. Mater. Sci. 29 (1999) 295–326.
[31] Y. Mizukoshi, K. Sato, T.J. Konno, N. Masahashi, Appl. Catal. B Environ. 94 (2010) 248–253.
[32] K. Okitsu, Theoretical and Experimental. Sonochemistry Involving Inorganic Systems, in: M. Ashokkumar (Ed.), Springer ScienceþBusiness Media, 2011, pp. 131–150.
[33] A. Cybula, J.B. Priebe, M.-M. Pohl, J.W. Sobczak, M. Schneider, A. Zielińska-Jurek, A. Brückner, A. Zaleska, Appl. Catal. B Environ. 152–153 (2014) 202–211.
[34] A. Sclafani, J.-M. Herrmann, J. Photochem. Photobiol. A Chem. 113 (1998) 181–188.
[35] A. Wold, Chem. Mater. 5 (1993) 280–283.
[36] R. Camposeco, S. Castillo, I. Mejía-Centeno, J. Navarrete, J. Marín, Mater. Charact. 95 (2014) 201–2010.
[37] J. Panpranot, K. Kontapakdee, P. Praserthdam, Appl. Catal. A Gen. 314 (2006) 128–133.
[38] L. Maffucci, P. Iengo, M. Di Serio, E. Santacesaria, J. Catal. 172 (1997) 485–487.
[39] S. Kalathil, M.M. Khan, A.N. Banerjee, J. Lee, M.H. Cho, J. Nanopart. Res. 14 (2012) 1051.
[40] P.V. Kamat, J. Phys. Chem. C 111 (2007) 2834–2860.
[41] A. Primo, A. Corma, H. García, Phys. Chem. Chem. Phys. 13 (2011) 886–910.
[42] X. Zhang, F. Wu, X. Wu, P. Chen, N. Deng, J. Hazard. Mater. 157 (2008) 300–307.
[43] L. Yang, L.E. Yu, M.B. Ray, Environ. Sci. Technol. 43 (2009) 460–465.
[44] H.C.A. Valdez, G.G. Jiménez, S.G. Granados, C.P. De León, Chemosphere 89 (2012) 1195–1201.
[45] J.-K. Im, L.K. Boateng, J.R.V. Flora, N. Her, K.-D. Zoh, A. Son, Y. Yoon, Sep. Purif. Technol. 123 (2014) 96–105.
[46] T.J. Mason, D. Peter, Practical Sonochemistry: Power Ultrasound Uses and Applications, 2nd ed., Horwood Chemical Science Series, 2002.
[47] G. Mark, M. Schuchmann, H.P. Schuchmann, C. Sonntag, J. Water Supply Res. Technol. 39 (1990) 309–313.
[48] N.V. Kiassen, D. Marchington, H.C.E. Mcgowant, Anal. Chem. 66 (1994) 2921–2925.
[49] K. Huang, R.A. Couttenye, G.E. Hoag, Chemosphere 49 (2002) 413–420.
[50] R. Su, R. Tiruvalam, Q. He, N. Dimitratos, L. Kesavan, C. Hammond, J.A. Lopez-sanchez, R. Bechstein, C.J. Kiely, G.J. Hutchings, F. Besenbacher, ACS Nano 6 (2012) 6284–6292.
[51] A.N. Ökte, D. Tuncel, A.H. Pekcan, T. Özden, J. Chem. Technol. Biotechnol. 89 (2014) 1155–1167.
[52] N.H. Ince, G. Tezcanli-Güyer, Ultrasonics 42 (2004) 591–596.
[53] N.H. Ince, I. Gültekin, G. Tezcanli-Güyer, J. Hazard. Mater. 172 (2009) 739–743.
[54] Z. Eren, N.H. Ince, J. Hazard. Mater. 177 (2010) 1019–1024.
[55] Q. Fu, T. Wagner, S. Olliges, H.D. Carstanjen, J. Phys. Chem. B 109 (2005) 944–951.
[56] L.-Y. Jin, R.-H. Ma, J.-J. Lin, L. Meng, Y.-J. Wang, M.-F. Luo, Ind. Eng. Chem. Res. 50 (2011) 10878–10882.
[57] F. Hao, W. Guo, A. Wang, Y. Leng, H. Li, Ultrason. Sonochem. 21 (2014) 554–558.
[58] A. Tsitonaki, B. Petri, M. Crimi, H. Mosbæk, R.L. Siegrist, P.L. Bjerg, Crit. Rev. Environ. Sci. Technol. 40 (2010) 55–91.
[59] D. Zhou, L. Ding, H. Cui, H. An, J. Zhai, Q. Li, J. Power Sources 222 (2013) 510–517.
[60] H. Hori, Y. Nagano, M. Murayama, K. Koike, S. Kutsuna, J. Fluorine Chem. 141 (2012) 5–10.
[61] X. Wang, L. Wang, J. Li, J. Qiu, C. Cai, H. Zhang, Sep. Purif. Technol. 122 (2014) 41–46.
[62] S. Su, W. Guo, C. Yi, Y. Leng, Z. Ma, Ultrason. Sonochem. 19 (2012) 469–474.

[63] P. Gayathri, R.P.J. Dorathi, K. Palanivelu, Ultrason. Sonochem. 17 (2010) 566–571.
[64] Y.-C. Lee, S.-L. Lo, J. Kuo, Y.-L. Lin, Chem. Eng. J. 198-199 (2012) 27–32.
[65] R. Su, R. Tiruvalam, Q. He, N. Dimitratos, L. Kesavan, C. Hammond, J.A. Lopez-sanchez, R. Bechstein, C.J. Kiely, G.J. Hutchings, F. Besenbacher, ACS Nano 6 (2012) 6284–6292.
[66] I.P. Pozdnyakov, X. Zhang, T. a. Maksimova, V.V. Yanshole, F. Wu, V.P. Grivin, V.F. Plyusnin, J. Photochem. Photobiol. A Chem. 274 (2014) 117–123.
[67] Y. Tian, T. Tatsuma, J. Am. Chem. Soc. 127 (2005) 7632–7637.
[68] Y. Wang, D.A.N. Zhao, W. Ma, C. Chen, J. Zhao, Environ. Sci. Technol. 42 (2008) 617.